Free Energy Relationship for Electron Transfer Far from Equilibrium. Analysis of Reversibility in the Endergonic Region

R. J. Klingler and J. K. Kochi*

Contribution from the Department of Chemistry, Indiana University, Bloomington, Indiana 47405. *Received September 10, 1981*

Abstract: Electron-transfer rate constants are measured over an extended range of the free energy change (ΔG) for a single system. Since the experimental free energy relationship encompasses both the exergonic and endergonic extremes, it dramatically emphasizes the existence of curvature that previously had been observed only over a much narrower span of ΔG. The kinetic measurements employ a cyclic voltammetric technique that allows the free energy change for electron transfer to be continuously tuned to the applied electrode potential E. The resulting free energy relationship for outer-sphere electron transfer from the organometal $Me_2Co(DpnH)$ exhibits a limiting behavior of the experimental transfer coefficient (β_e), which approaches 0 in the exergonic limit and 1 in the endergonic limit, as shown in Figure 3. Kinetic and error analyses of the electrochemical technique demonstrate that in the exergonic region [i.e., as one proceeds beyond $E^\circ = 0.53$ V for $Me_2Co(DpnH)$], the *experimental* rate constant k_e represents an accurate representation of the *intrinsic* rate constant k_1 for electron transfer. However, as one drops into the endergonic region below 0.53 V, the reversibility in the electron-transfer step becomes increasingly more important, and k_e can only be explicitly related to k_1 by specifically taking into account the decomposition rate constant k_2 of the organometal cation. The general kinetic solution given in eq 10 then allows the intrinsic rate constant k_1 to be determined in the endergonic region. It is noteworthy that the excellent fit of the resulting rate data to the Rehm–Weller free energy relationship can be achieved with a single value of the intrinsic barrier ΔG_0^* over the entire span of the free energy change. The evaluation of the standard reduction potentials for irreversible systems is described in the context of the Marcus theory for outer-sphere electron transfer.

The Marcus theory of electron transfer has provided a quantitative means of analysis of outer-sphere mechanisms.[1-3] It is particularly useful for predicting electron-transfer rates near the equilibrium potential, such as the self-exchange processes. However, its applicability decreases as the free energy change is removed from this benchmark. Although several empirical free energy relationships are known,[4-7] no adequate theory exists for the description of the energy gamut that simultaneously includes the exergonic as well as the endergonic limits.[8-11]

The desirability of an extended free energy relationship stems from its importance to systems that undergo interesting chemistry attendant upon electron transfer. These include an ever increasing number and variety of organic and organometallic systems in which questions relating to the involvement of (single) electron transfer or "SET" mechanisms have arisen.[12] For these chemically irreversible systems, electron-transfer rates are often measureable only at potentials far removed from equilibrium.[13,14]

A basic experimental challenge is thus to establish the functional dependence of the rate of electron transfer over an extended region of the free energy change (ΔG). Most of the electron-transfer studies have heretofore been carried out in homogeneous systems in which the chemical oxidants and reductants are both in solution.[15] Such homogeneous studies are circumscribed by the availability of chemical oxidants and reductants with standard reduction potentials sufficient to span only a limited range of ΔG.[8] Furthermore, varying structures with different steric properties as well as changing magnitudes of the reorganization energies must be employed to encompass an extended span. Thus there are advantages to be gained in the study of a *single* system over a wide range of ΔG. Electrochemical oxidation and reduction provide such an opportunity, and it is somewhat surprising that only a limited number of systems have been examined with this end in mind. In particular, the electrochemical EC mechanism outlined in the simple kinetic Scheme I is an especially viable one for covering wide ranges in the free energy change. For example,

(1) Marcus, R. A. *J. Phys. Chem.* **1963**, *67*, 853.
(2) Marcus, R. A. *Annu. Rev. Phys. Chem.* **1964**, *15*, 155.
(3) Marcus, R. A. In "Tunneling in Biological Systems"; Chance, B., et al., Eds.; Academic Press: New York, 1979; p 109 ff.
(4) Rehm, D.; Weller, A. *Ber. Bunsenges. Phys. Chem.* **1969**, *73*, 834. *Isr. J. Chem.* **1970**, *8*, 259.
(5) Marcus, R. A. *J. Phys. Chem.* **1968**, *72*, 891.
(6) Evans, M. D.; Polanyi, M. *Trans. Faraday Soc.* **1936**, *32*, 1340. **1938**, *34*, 11.
(7) (a) For a current assessment of free energy relationships in electron transfer, see: Scandola, F.; Balzani, V.; Schuster, G. B. *J. Am. Chem. Soc.* **1981**, *103*, 2519. (b) Free energy relationships, also referred to as rate–equilibrium relationships and structure–reactivity correlations, have also been quantitatively treated for other types of reactions in a more general context. For summaries, see: (c) Murdoch, J. R. *Ibid.* **1972**, *94*, 4410. (d) Agmon, N. *Int. J. Chem. Kinet.* **1981**, *13*, 333.
(8) The lack of a theoretical model arises, at least in part, from the scarcity of reliable experimental data for systems far removed from the equilibrium potential. Indeed the concentration of the electron-transfer literature for systems at or close to the equilibrium potential is often dictated by experimental considerations. Thus the measurements of electron-transfer rates of substitution-stable oxidants and reductants are most conveniently carried out at the equilibrium potentials, both in homogeneous chemical and heterogeneous electrode processes.[9-11]
(9) (a) Reynolds, W. L.; Lumry, R. W. "Mechanisms of Electron Transfer"; Ronald Press: New York, 1966. (b) Delahay, P. "The Electric Double Layer and Electrode Kinetics"; Interscience: New York, 1965.
(10) (a) Reinmuth, W. H. *Anal. Chem.* **1964**, *36*, 211R. (b) Vetter, K. J. "Electrochemical Kinetics"; Academic Press: New York, 1967.
(11) (a) Pletcher, D. *Chem. Soc. Rev.* **1975**, *75*, 1190. (b) Streitwieser, A. In "Physical Methods in Chemistry"; Weissberger, A., Rossiter, B. W., Eds.; Wiley: New York, 1971; Part IIa. (c) Schmidt, P. P. *Electrochemistry* **1975**, *5*, 21. **1976**, *6*, 128.
(12) (a) The vogue among some is to refer to organic and organometallic mechanisms that proceed via electron transfer as single electron transfer or SET. (b) For examples of electron transfer in such processes, see: Kochi, J. K. "Organometallic Mechanisms and Catalysis"; Academic Press: New York, 1978. Ashby, E. C.; Goel, A. B.; DePriest, R. N.; Prasad, H. S. *J. Am. Chem. Soc.* **1981**, *103*, 973, and related papers. Bordwell, F. G.; Clemens, A. H. *J. Org. Chem.* **1981**, *46*, 1035. Chanon, M. *Angew. Chem.* **1982**, *21*, 1. A wide variety of photochemical processes involving electron transfer in the quenching of excited states is also known. For some leading references, see: Geofroy, G. L.; Wrighton, M. S. "Organometallic Photochemistry"; Academic Press: New York, 1979. Adamson, A. W.; Fleischauer, P. D., Eds; "Concepts of Inorganic Photochemistry"; Wiley: New York, 1975.
(13) For systems in which reduction potentials are known, see: (a) Andrieux, C. P.; Blocman, C.; Dumas-Bouchiatt, J. M.; Saveant, J. M. *J. Am. Chem. Soc.* **1979**, *101*, 3431. (b) Klingler, R. J.; Kochi, J. K. *Ibid.* **1980**, *102*, 4790.
(14) For systems in which reduction potentials are not established, see: (a) Schuster, G. B. *J. Am. Chem. Soc.* **1979**, *101*, 5851 and references therein. Scandola, F.; Balzani, V.; Schuster, G. B. *Ibid.* **1981**, *103*, 2519. (b) For the kinetic ambiguity, see: Walling, C. *Ibid.* **1980**, *102*, 6854.
(15) Cannon, R. D. "Electron-Transfer Reactions"; Butterworths: Boston, 1980.

0002-7863/82/1504-4186$01.25/0

Scheme I

$$A \underset{k_{-1}}{\overset{k_1}{\rightleftharpoons}} A^+ + e \quad (1)$$

$$A^+ \xrightarrow{k_2} \text{product} \quad (2)$$

the rate of the forward electron transfer in eq 1 is readily and continuously tuned by the applied electrode potential over a wide range, the relationship simply being[16]

$$k(E) = k_s \exp\left[\frac{\beta n \mathcal{F}}{RT}(E - E^\circ)\right] \quad (3)$$

where E is the electrode potential, n is the number of electrons transferred from the electroactive species A in the rate-limiting step, β is the transfer coefficient for the electrode process, and E° is the standard reduction potential, which fixes the value of k_s, the standard rate constant. $\mathcal{F}$ is the Faraday constant, and R and T have their usual significance. Although Scheme I illustrates the kinetics of the oxidation of the electroactive species A, the same basic notion applies, of course, to its reduction. The use of transient electrochemical techniques such as the readily available cyclic voltammetry allows the rate of the followup process to be varied simply by altering the sweep rate.[17] Thus the degree of reversibility in eq 1 is an experimental variable that can be examined over a wide range of electron-transfer rates.

In previous studies we have shown how organometals are ideally suited to be utilized as electron donors in electrochemical EC systems.[18] Among the various organometals examined, the organocobalt macrocycle typified by $Me_2Co(DpnH)$[19,20]

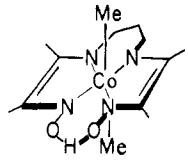

is unusually well-suited in that the essential kinetic features of Scheme I have all been verified. Thus, the first-order decay of the radical cation $A^+ = Me_2Co(DpnH)^+$ proceeds with the rate constant $k_2 = 10^5\ s^{-1}$. The zero-order dependence on the unoxidized species $A = Me_2Co(DpnH)$ has been demonstrated, and the distinction between a one- and two-electron electrode process has been established by competition kinetics with suitable trapping methods.[19] In addition, the direct comparison with electron transfer effected by various chemical oxidants in solution has delineated the fundamental unity of outer-sphere electron transfer between heterogeneous electrochemical and homogeneous chemical processes in these systems.[13b] This large body of mechanistic information is unusually valuable since it now provides us with the necessary support to focus on the measurement of the rates of electron transfer over an extended range of the free energy change, i.e., the applied electrode potential E.[21] We wish to show how the resulting potential dependence of the rate bears critically on the free energy relationships for electron transfer, especially as they are affected by the reversibility in Scheme I. The evaluation of the transfer coefficient β forms an important basis of this analysis.[22]

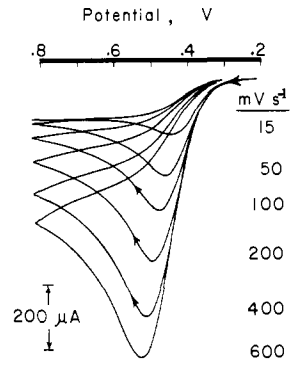

Figure 1. Single-scan cyclic voltammogram of 3.3×10^{-3} M $Me_2Co(DpnH)$ in acetonitrile solutions containing 0.1 M TEAP at various scan rates. Electrode potentials in volts vs. saturated NaCl SCE.

Results

The experimental determination of the electron-transfer rates derives from the cyclic voltammetric technique described in detail for $Me_2Co(DpnH)$. The free energy correlation of the experimental rate constant k_e is then established over an extended range of the free energy change for this system.

Cyclic Voltammetry of $Me_2Co(DpnH)$. The cyclic voltammograms (CV) of $Me_2Co(DpnH)$ were recorded at 25 °C with a stationary platinum microelectrode in acetonitrile solutions containing 0.1 M tetraethylammonium perchlorate (TEAP). The initial positive scan cyclic voltammogram illustrated in Figure 1 is characterized by an anodic wave showing a well-defined current maximum but no coupled cathodic wave on the reverse scan, even at sweep rates up to $10^3\ V\ s^{-1}$ and at temperatures as low as −80 °C. A closer inspection of the details of the sweep dependence reveals that the current in the initial portion (i.e., foot) of the CV wave is singularly independent of the sweep rate. The foot of an electrochemical wave represents an important limiting situation in which the concentration of the electroactive species is effectively constant and equal to that in the bulk solution. Thus the current in the earliest portion of the CV wave may be analyzed solely on the basis of the electron-transfer process, without reference to diffusion of the reactants to the electrode.[23] Indeed the lack of dependence of the current on the sweep rate for a considerable portion of the foot (see Figure 1) confirms the net forward rate of electron transfer from $Me_2Co(DpnH)$ to be independent of the diffusion of the products away from the electrode surface. (Note that the rate of diffusion is known to be proportional to the square root of the sweep rate.[24]) Kinetically such a situation would arise in Scheme II if the decomposition of the oxidized $Me_2Co(DpnH)$ in eq 5 were more facile than the reverse rate of electron transfer in eq 4, where M = DpnH.[19,20] Inspection of the CV curves in

Scheme II

$$Me_2CoM \underset{k_{-1}}{\overset{k_1}{\rightleftharpoons}} Me_2CoM^+ + e \quad (4)$$

$$Me_2CoM^+ \xrightarrow{k_2} Me\cdot + MeCoM^+, \text{ etc.} \quad (5)$$

Figure 1 also reveals a peak broadening that accompanies the increasing sweep rates. The nature of this apparent change in electrochemical reversibility is described in detail in the Experimental Section.

(16) Bauer, H. H. *J. Electroanal. Chem. Interfacial Electrochem.* **1968**, *16*, 419.

(17) The followup process consists of the sum of the homogeneous rate constant k_2 for the decomposition of A^+ and the diffusion of A^+ from the electrode surface. Altering the sweep rate changes the diffusion rate. See: Galus, Z. "Fundamentals of Electrochemical Analysis"; Wiley: New York, 1976.

(18) Klinger, R. J.; Kochi, J. K. *J. Phys. Chem.* **1981**, *85*, 1731, and ref 13b.

(19) Tamblyn, W. H.; Klingler, R. J.; Hwang, W. S.; Kochi, J. K. *J. Am. Chem. Soc.* **1981**, *103*, 3161.

(20) DpnH = 2,3,9,10-tetramethyl-1,4,8,11-tetraazaundeca-1,3,8,10-tetracen-11-ol-1-olate.

(21) For electron-transfer processes, note that the variation in the applied potential E at an electrode is equivalent to using a graded series of oxidants (or reductants) with different standard potentials E° in a homogeneous chemical process. The driving force or free energy change is then given by $\Delta G = -n\mathcal{F}(E - E^\circ)$.

(22) In electrochemical kinetics, the dependence of the rate constant on the driving force is usually referred to as the *transfer* coefficient β, which in homogeneous chemical kinetics is generally designated as the *Brønsted* coefficient α.

(23) Reinmuth, W. H. *Anal. Chem.* **1960**, *32*, 1891.

(24) Adams, R. W. "Electrochemistry at Solid Electrodes"; Dekker: New York, 1969.

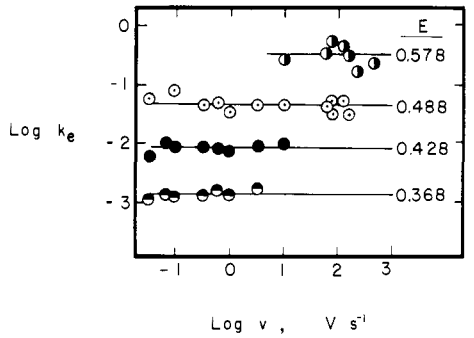

Figure 2. The constancy of the experimental rate constant k_e for electron transfer with the variation in the CV sweep rate at E = 0.578, 0.488, 0.428, and 0.368 V vs. saturated NaCl SCE.

To evaluate the kinetic situation in Scheme II quantitatively we now make a rigorous conversion of the current–potential profiles in Figure 1 to the rate constant k_e for the *net forward* electron transfer at the various electrode potentials, i.e., the free energy changes.

Evaluation of the Heterogeneous Rate Constants for Electron Transfer from the Cyclic Voltammogram. The heterogeneous rate constant for the net forward electron transfer is proportional to the electrochemical current. At a given applied potential E, the rate constant k_e is related to the current $i(E)$ by the expression[25]

$$k_e(E) = i(E)/[n\mathcal{F}AC(t)] \quad (6)$$

where A is the area of the electrode and $C(t)$ is the time-dependent concentration of the electroactive species (i.e., $Me_2Co(DpnH)$) at the electrode surface. The values of $C(t)$ can be evaluated from the current–time history by using the convolution integral[26]

$$C(t) = C^0\left[1 - \frac{10^3}{n\mathcal{F}AC^0(\pi D)^{1/2}}\int_0^t \frac{i(\eta)}{(t-\eta)^{1/2}}\,d\eta\right] \quad (7)$$

where C^0 is the initial concentration of $Me_2Co(DpnH)$ in the bulk solution, as described in detail in the Experimental Section. It is important to emphasize that eq 7 is kinetically rigorous since it derives directly from Fick's laws of diffusion.[27] The validity of eq 7 is independent of the nature or complexity of the kinetic scheme provided the only means of depleting (or of increasing) the total amount of electroactive species involves the transfer of charge—in other words, the current $i(E)$ must be faradaic. It pertains to cases such as that in Scheme II in which the electroactive species are thermally stable and are not catalytically regenerated via a nonfaradaic pathway from the products of electrolysis.[19] The use of eq 6 and 7 thus allows values of the rate constants k_e for heterogeneous electron transfer to be evaluated from the current–potential data contained in the cyclic voltammogram. In practice, the faradaic current is obtained from the observed current after correction for the charging current. Since the charging current increases linearly with the sweep rate, in contrast to a square-root dependence of the faradaic current with sweep rate, the error in the measurement of the faradaic current increases with the sweep rate. As a result, the observed current as well as the charging current must be measured precisely under the same conditions, particularly at high sweep rates. A detailed description of the experimental procedure is given separately in the Experimental Section. Table I summarizes typical values of the experimental rate constant k_e obtained at various applied potentials E. A more extended list of k_e and E, including all the data employed in this study, is tabulated in the supplementary material.

(25) Delahay, P. "New Instrumental Methods in Electrochemistry"; Interscience: New York, 1954.
(26) Saveant, J. M.; Tessier, D. *J. Phys. Chem.* **1978**, *82*, 1723. Note that eq 7 and 25 in ref 49 should be corrected to those given here. A factor of 10^3 has also been omitted in eq 7 of ref 27.
(27) Imbeaux, J. C.; Saveant, J. M. *J. Electroanal. Chem. Interfacial Electrochem.* **1973**, *44*, 169.

Table I. Heterogeneous Rate Constants for Electron Transfer from $Me_2CO(DpnH)$ by Convolutive Potential Sweep Voltammetry[a]

v,[b] V s^{-1}	$i(E)$, mA	i_c, mA[c]	E, V[d]	log k_e, cm s^{-1}	log k_l, cm s^{-1}
0.03	0.0092	0.0004	0.318	−3.6800	−3.1969
0.03	0.0212	0.0004	0.347	−3.2700	−2.9171
0.03	0.0406	0.0004	0.373	−2.8900	−2.6028
0.03	0.0603	0.0004	0.399	−2.5600	−2.3559
0.03	0.0688	0.0004	0.421	−2.3000	−2.1518
0.06	0.0287	0.0007	0.356	−3.0600	−2.6223
0.06	0.0914	0.0007	0.416	−2.1800	−1.9097
0.10	0.0412	0.0026	0.368	−2.9300	−2.5962
0.10	0.0936	0.0028	0.406	−2.3900	−2.1519
0.30	0.0315	0.0079	0.346	−3.2100	−2.7361
0.30	0.0745	0.0096	0.383	−2.7200	−2.4323
0.30	0.1485	0.0086	0.414	−2.2700	−2.0430
0.30	0.2155	0.0107	0.446	−1.8800	−1.7333
0.60	0.0555	0.0079	0.361	−2.9100	−2.3283
0.60	0.2540	0.0095	0.437	−1.9700	−1.7954
1.00	0.0790	0.0152	0.377	−2.7900	−2.4703
1.00	0.1840	0.0169	0.416	−2.3000	−2.1120
1.00	0.3540	0.0181	0.460	−1.8000	−1.7033
3.00	0.0890	0.0244	0.368	−2.7800	−2.1647
3.00	0.2070	0.0144	0.409	−2.2600	−1.9534
3.00	0.3430	0.0178	0.435	−1.9800	−1.7931
3.00	0.6070	0.0261	0.476	−1.5200	−1.4211
3.00	0.6980	0.0283	0.501	−1.2500	−1.1830
10.00	0.2920	0.0564	0.412	−2.2000	−1.8838
10.00	0.5280	0.0588	0.441	−1.8500	−1.6470
10.00	0.8380	0.0624	0.472	−1.5300	−1.4150
10.00	1.06	0.07	0.495	−1.3000	−1.2238
10.00	1.24	0.07	0.525	−1.0100	−0.9655
1000.00	3.40	3.30	0.534	−0.9500	−0.9144
1000.00	3.84	3.74	0.568	−1.4500	−1.4471
800.00	3.94	3.40	0.620	−0.6200	−0.6174
666.00	3.68	3.22	0.610	−0.4300	−0.4241
500.00	3.33	2.85	0.626	0.800	0.0902
300.00	1.58	1.30	0.514	−1.5400	−1.5204
225.00	2.25	1.16	0.588	−0.7200	−0.7129
225.00	1.65	1.01	0.540	−1.1000	−1.0804
175.00	1.41	0.83	0.530	−1.1200	−1.0921
175.00	2.27	0.88	0.596	−0.4500	−0.4403
175.00	2.20	0.86	0.590	−0.5100	−0.4993
143.00	2.11	0.73	0.608	−0.1900	−0.1789
143.00	2.10	0.72	0.596	−0.3200	−0.3068
114.00	0.7420	0.5002	0.468	−1.5300	−1.3922
114.00	1.77	0.60	0.586	−0.3500	−0.3317
114.00	1.67	0.54	0.566	−0.4400	−0.4071
89.00	0.8140	0.4422	0.492	−1.2600	−1.1639
89.00	0.7760	0.4377	0.482	−1.6200	−1.5605
89.00	1.38	0.48	0.542	−0.6700	−0.6195
89.00	1.21	0.44	0.524	−0.8200	−0.7459
67.00	0.5540	0.3784	0.472	−1.6900	−1.6138
67.00	1.20	0.44	0.554	−0.7900	−0.7668
67.00	0.4840	0.3656	0.458	−1.8600	−1.7696
67.00	0.7640	0.3936	0.502	−1.2900	−1.2318
67.00	1.18	0.43	0.548	−0.8000	−0.7711
67.00	0.5300	0.3564	0.464	−1.6800	−1.5693
67.00	1.19	0.41	0.540	−0.7800	−0.7380

[a] In acetonitrile solution containing 0.1 M tetraethylammonium perchlorate at 25 °C. [b] Sweep rate. [c] Charging current. [d] Applied potential vs. saturated NaCl SCE.

The results in Figure 2 demonstrate that the rate constants (log k_e) obtained in this manner are indeed independent of the sweep rate (log v), varied over 4.2 orders of magnitude. The four values of the applied potential were arbitrarily chosen to cover the entire breadth of the CV waves in Figure 1. Note that the scatter in the data is more pronounced at the faster sweep rates, owing to the larger errors in the measurement of the faradaic current described above.

The rate constant at a particular potential was obtained by averaging the values obtained at various sweep rates, and it is plotted against the applied potential E in Figure 3. The smooth variation covers a span of 2×10^3 in the rate constant and a span of more than 0.4 V in the free energy change for heterogeneous

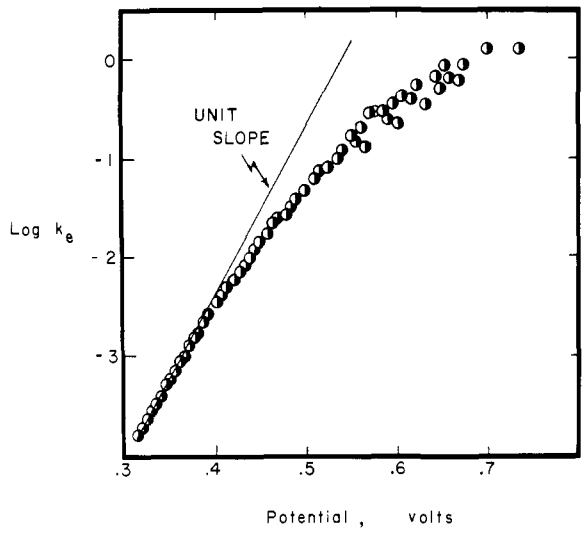

Figure 3. The variation in the experimental rate constant k_e for electron transfer as a function of applied potential (free energy change). The limiting slope in the endergonic region is shown by the fit to the line arbitrarily drawn with a slope of unity. For a direct comparison of log k_e and the potential, a multiplicative factor of $2.3RT/\mathcal{F}$ must be included.

electron transfer.[28] Two features are noteworthy in Figure 3. First, at the low-potential end, the limiting slope of the relationship between the activation free energy (log k_e) and the applied potential (E) is close to unity, as shown by the line of unit slope included in Figure 3. Second, at the other limiting extreme, of high potential, the net forward rate constant for electron transfer is observed to be clearly leveling off and *becoming* independent of the applied potential. At this juncture it is important to emphasize that the intermediate slope of 0.5 occurs in Figure 3 as a tangent at only the *middle* (E = 0.53 V) of an obvious curve. Therefore from a strictly graphical or mechanical point of view, 0.5 cannot possibly represent a limiting value of the slope in this system. The variation of the experimental rate constant k_e for electron transfer is thus clearly nonlinear over the extended range of the free energy change in Figure 3.

Discussion

The electron-transfer rate behavior so graphically illustrated in Figure 3 is unique, and we know of no other kinetic measurement in which both limiting kinetic extremes have been covered, particularly in a single system. Consequently, we now wish to exploit the experimental information contained in Figure 3 to develop the free energy relationship for electron transfer over an extended range. To determine the functional dependence of the rate constant for electron transfer with the free energy change, we must first clearly delineate the distinction between the *experimental* rate constant k_e and the *intrinsic* rate constant k_1 for forward electron transfer in Scheme I. Indeed, the relationship between the two rate constants is critically dependent on the lifetime of the electrogenerated intermediate A^+, which is determined from the magnitudes of the rate constant k_{-1} for back electron transfer and the rate constant k_2 for decomposition, as graphically illustrated here.

$$A \underset{k_{-1}}{\overset{k_1}{\rightleftharpoons}} e + A^+ \xrightarrow{k_2} \text{product} \qquad (k_e)$$

The rigorous combination of the kinetics of Scheme I with Fick's laws of diffusion affords the relationship among these rate constants:

$$k_e = k_1[k_2'/(k_{-1} + k_2')] \qquad (8)$$

(28) For the significance of these numbers, they should be considered in light of the small reorganization energy $4\Delta G_0^*$ for $Me_2Co(DpnH)$. See eq 12–14 and 21.

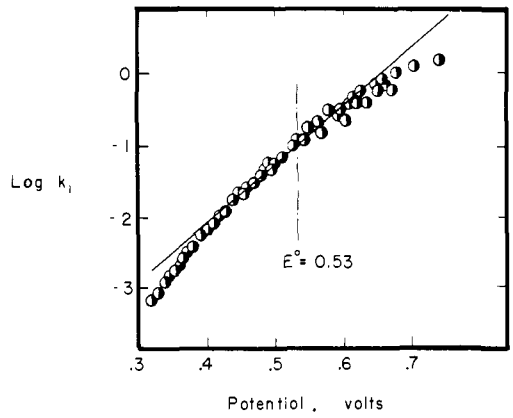

Figure 4. Free energy relationship for the intrinsic electron-transfer rate constant k_1 obtained from the experimental rate constant k_e after correction for reversibility according to eq 10. The line represents $\beta = {}^1/_2$, and E° is determined as described in the text. For a direct comparison of log k_e and the potential, a multiplicative factor of $2.3RT/\mathcal{F}$ must be included.

which is the same as that obtained from a straightforward steady-state treatment.[29] (Note that the homogeneous rate constant k_2 in Scheme I has been converted to its heterogeneous equivalent k_2' for use in eq 8.[31])

Evaluation of the Intrinsic Rate Constant k_1 for Electron Transfer. The evaluation of the intrinsic rate constant k_1 proceeds from the rearrangement of eq 8:

$$k_1 = k_e k_2' \left(k_2' - k_e \frac{k_{-1}}{k_1} \right)^{-1} \qquad (9)$$

followed by the combination with the Nernst expression[32] to yield eq 10. The complete kinetic expression in eq 10 relates the

$$k_1 = k_e k_2' \left\{ k_2' - k_e \exp\left[\frac{-n\mathcal{F}}{RT}(E - E^\circ) \right] \right\}^{-1} \qquad (10)$$

experimental rate constant k_e with the forward rate constant k_1 for electron transfer as a direct function of the decomposition rate constant k_2' and the standard reduction potential E^0. Since an independent measurement of k_2' = 1.2 cm s^{-1} or $k_2 = 10^5$ s^{-1} is available for $Me_2Co(DpnH)^+$ from the previous study,[19] it can be used in conjunction with E° = 0.53 V[33] to convert the experimental k_e listed in Table I to the intrinsic rate constant k_1 for forward electron transfer in Scheme I. The results of the kinetic analysis for the intrinsic rate constant k_1 based on eq 10 are replotted in Figure 4.

(29) Owing to the constraints of the Nernst equation, Scheme I actually contains only two independent rate constants at any particular value of the applied potential. Thus the general kinetic analysis may be discussed in terms of a two-dimensional diagram and the parameters most conveniently chosen as k_2 and k_s. (The latter is defined by eq 3.) A detailed analysis of this two-dimensional grid has been performed by Nadjo and Saveant,[30] who identified six kinetic possibilities or zones. We have shown that the steady-state model in eq 8 is generally applicable, by calculations performed in each of these six zones (see the Experimental Section).[18] Saveant's analysis was also extended by treating the sensitivity to the applied potential (i.e., β) as an additional or third parameter in the confirmation of the steady-state expression. Thus the validity of eq 8 is not dependent on simplifying assumptions, such as those made in the classical reaction-layer method.

(30) Nadjo, L.; Saveant, J. M. *J. Electroanal. Chem. Interfacial. Electrochem.* **1973**, *48*, 113.

(31) The relationship is $k_2' = (Dk_2)^{1/2}$, where $D = 1.5 \times 10^{-5}$ cm^2 s^{-1} is the diffusion coefficient of $Me_2Co(DpnH)$.[19] The comparison of the heterogeneous rate process (k_{-1}) with the homogeneous decay (k_2) as in Scheme I requires the intervention of a third rate process, i.e., mass transport. See ref 17 for additional elaborations of this point.

(32) Bard, A. J.; Faulkner, L. R. "Electrochemical Methods"; Wiley: New York, 1980.

(33) (a) To avoid discontinuity of the discussion at this juncture, the theoretical basis for the evaluation of E° is presented separately in the last part of this paper. (b) The general applicability of this criterion for the determination of the standard electrode potential rests on the independent verification of the kinetics in Scheme I as it applies to $Me_2Co(DpnH)$.[19]

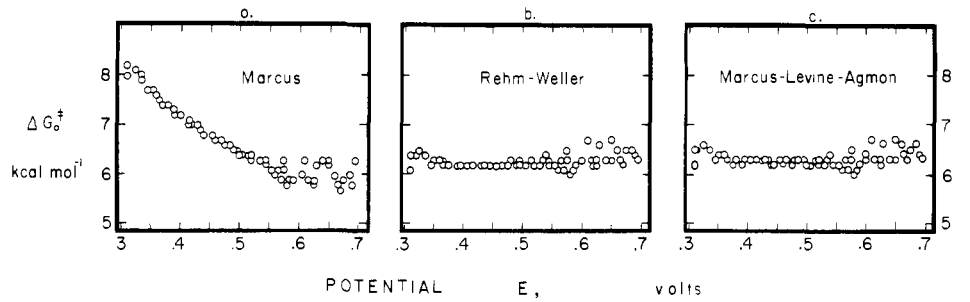

Figure 5. Consistency of the intrinsic barrier $\Delta G_0^{\ddagger}$ evaluated from the intrinsic rate constant (log k_1) by using (a) Marcus eq 12, (b) Rehm–Weller eq 13, and (c) Marcus–Levine–Agmon eq 14 at various potentials.

The curve in Figure 4 encompasses as extensive a span of potentials as possible for a single system. Most importantly, it underscores the important observation of curvature in the relationship between the intrinsic rate constant (log k_1) and the applied potential. Since the latter is directly related to the experimental free energy change ΔG for electron transfer,[21] the plot in Figure 4 represents an experimental determination of the free energy relationship for electron transfer over an extended region of the free energy change. Our problem now is to determine the functional form of this experimental free energy curve.

Functional Dependence of the Intrinsic Rate Constant k_1 on the Free Energy Change. Experimental Tests of Various Free Energy Relationships. The rate constant k_1 for an outer-sphere electron transfer is given in eq 11, where $\Delta G^{\ddagger}$ is the free energy of activation

$$k_1 = Z \exp(-\Delta G^{\ddagger}/RT) \qquad (11)$$

and the collision frequency Z is taken as 3.5×10^3 cm s^{-1}.[34] Three different relationships are currently in use to relate the activation free energy to the free energy change[21] in electron-transfer reactions.

Marcus[1]

$$\Delta G^{\ddagger} = \Delta G_0^{\ddagger}\left[1 + \frac{\Delta G}{4\Delta G_0^{\ddagger}}\right]^2 \qquad (12)$$

Rehm–Weller[4]

$$\Delta G^{\ddagger} = \frac{\Delta G}{2} + \left[\left(\frac{\Delta G}{2}\right)^2 + (\Delta G_0^{\ddagger})^2\right]^{1/2} \qquad (13)$$

Marcus–Levine–Agmon[5,35]

$$\Delta G^{\ddagger} = \Delta G + \frac{\Delta G_0^{\ddagger}}{\ln 2} \ln\left[1 + \exp\left(-\frac{\Delta G \ln 2}{\Delta G_0^{\ddagger}}\right)\right] \qquad (14)$$

Each of these free energy relationships employs the intrinsic barrier $\Delta G_0^{\ddagger}$ as the disposable parameter. [The intrinsic barrier represents the activation energy for electron transfer when the driving force is zero, i.e., $\Delta G^{\ddagger} = \Delta G_0^{\ddagger}$ at $\Delta G = 0$ or the equilibrium potential E°.] Since the intrinsic barrier is the single parameter in eq 12, 13, and 14, the applicability of these relationships to the experimental free energy curve in Figure 4 is best carried out by testing each for the consistency of $\Delta G_0^{\ddagger}$, which was calculated from the experimental value of $\Delta G^{\ddagger}$ at each ΔG. The result is graphically illustrated in Figure 5. Several features in Figure 5 are noteworthy. First, in the equilibrium region of $E^{\circ} = 0.53$ V,[33] all three relationships yield a consistent value of the intrinsic barrier as $\Delta G_0^{\ddagger} = 6.3$ kcal mol^{-1}. [Note that the scatter of points in the exergonic region arises from the experimental difficulties in the measurement of k_e (vide supra).] Second, the applicability of the Marcus eq 12 is limited to the region of the free energy change about the equilibrium potential.[36] Significant deviations occur in the endergonic region, particularly at potentials less than ~0.4 V. Third, the Rehm–Weller and the Marcus–Levine–Agmon relationships are equally applicable over the entire span of the experimental free energy change. Both relationships yield values of $\Delta G_0^{\ddagger}$ that deviate less than 0.3 kcal mol^{-1} only at the extrema. This test thus represents a unique example of the experimental verification of these free energy relationships over an unusually extended range of the driving force.[37] Owing to its simpler functional form, all subsequent discussions of the free energy relationship for electron transfer will be based on the Rehm–Weller relationship.[38]

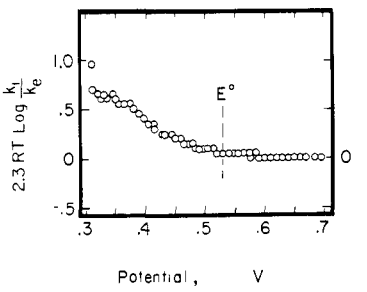

Figure 6. Comparison of the experimental rate constant k_e and the intrinsic rate constant k_1 at various potentials. The ordinate also represents an error expressed in units of kcal mol^{-1}.

Comparison of the Experimental Rate Constant k_e and the Intrinsic Rate Constant k_1. The Discrepancy in the Endergonic Region. The general kinetic expression in eq 10 allows the intrinsic rate constant k_1 to be evaluated from a knowledge of the experimental rate constant k_e by explicitly taking into account the reversibility in the electron-transfer step according to Scheme I. We must now ask how the magnitudes of k_e and k_1 differ, particularly over the entire span of the driving force. Unfortunately, the experimental curve for the rate constant k_e (Figure 3) is not readily distinguished from the curve for the intrinsic rate constant k_1 (Figure 4) by a mere visual comparison. Thus a more descriptive approach to this problem is presented in Figure 6 in which the ratio of the intrinsic and experimental rate constants, i.e., log k_1/k_e, is plotted against the potential. Two regions of the free energy change can now be readily identified in Figure 6.

(i) For potentials greater than ~0.4 V, the experimental rate constant k_e is indeed an excellent measure of the intrinsic rate constant k_1. In particular, for the exergonic region beyond 0.53 V, the relationship is given by eq 15. This relationship also

$$\text{Irreversible Case:} \quad k_e = k_1 \qquad (15)$$

(34) See: Saveant, J. M.; Tessier, D. *J. Phys. Chem.* **1977**, *81*, 2192, and ref 18.

(35) Levine, R. D. *J. Phys. Chem.* **1979**, *83*, 159. Agmon, N.; Levine, R. D. *Chem. Phys. Lett.* **1977**, *52*, 197. See also: Scandola, F.; Balzani, V.; Schuster, G. B., in ref 7a.

(36) Deviations from the Marcus eq 12 at large driving forces have been noted previously in a variety of homogeneous systems.

(37) The Rehm–Weller equation represents a true hyperbolic function of $\Delta G^{\ddagger}$ and ΔG. The Marcus–Levine–Agmon relationship follows a similar functional form but differs slightly at large values of $|\Delta G|$. The latter predicts that the rate constant for the anodic process of A will be slightly different than that for the cathodic process of A^+, when they are evaluated at the same driving force.

(38) (a) We have also used the Rehm–Weller equation here, since it has been successfully employed to fit the activation energies to an extended region of the driving force in other systems. See: (b) Scandola, F.; Balzani, V. *J. Am. Chem. Soc.* **1979**, *101*, 6140 and ref 11–18 cited therein. (c) Kresge, A. J. *Chem. Soc. Rev.* **1923**, *2*, 245. (d) Reference 34.

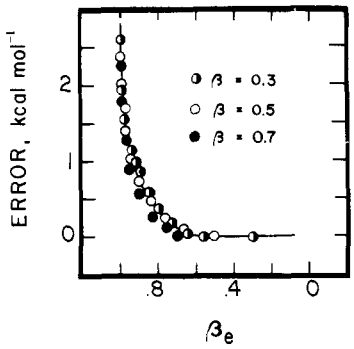

Figure 7. The relationship between transfer coefficient β_e and the error in evaluating the experimental rate constant k_e as the intrinsic rate constant k_1 for electron transfer according to eq 16.

represents the *irreversible* region of the kinetics since it follows from eq 8 when reverse electron transfer is nil, i.e., $k_{-1} \ll k_2'$.

(ii) For potentials less than ~0.4 V, the experimental rate constant k_e becomes an increasingly inadequate measure of the intrinsic rate constant k_1. Indeed the discrepancy between these rate constants can be expressed as an error function, i.e.,

$$\text{error} = 2.3RT(\log k_1 - \log k_e) \qquad (16)$$

The error thus defines the discrepancy between the experimental rate constant ($\log k_e$) and the intrinsic rate constant ($\log k_1$) in Scheme I as an energy difference in kcal mol^{-1}. We wish to describe how the discrepancy in the endergonic region of Figure 6 arises from the reversibility in the electron-transfer step.

Quantitative Analysis of Reversibility in the Electron-Transfer Step in the Endergonic Region. To understand the origin of the discrepancy between k_e and k_1 in Figure 6, we note that the error increases as one proceeds further into the endergonic region. Importantly, this trend also coincides with the approach to unit slope in the experimental free energy curve in Figure 3. Therefore, let us now focus on the significance of the slope in the free energy curve.

For heterogeneous electron-transfer processes, reversibility has traditionally been discussed in terms of the magnitude of the experimental transfer coefficient β_e, defined as the tangent to the experimental curve, such as that in Figure 3; i.e.:

$$\beta_e = \frac{2.3RT}{n\mathcal{F}} \frac{\partial \log k_e}{\partial E} \qquad (17)$$

In particular, the observation of β_e less than unity has been attributed to irreversibility in electron transfer.[39] Accordingly, the potential region above ~0.4 V in Figure 3 is consistent with irreversibility since the deviation from the line commences about there. Such an irreversibility based on a value of β_e accords with the conclusion in eq 15. Indeed we have recently extended this type of analysis by showing quantitatively how the experimental transfer coefficient β_e does provide a definitive error limit in the application of eq 15 to any real system.[18] The results of extensive computations show that the error as defined by eq 16 is a smooth function of the magnitude of the transfer coefficient β_e, as summarized in Figure 7. (The reader is encouraged to consult the original article, ref 18, for details of the analysis.) It is important to emphasize that the utility of the experimental β_e as an indicator of the error is independent of the magnitude of the intrinsic transfer coefficient β,[40] which is evaluated at 0.3, 0.5, and 0.7 in Figure 7.

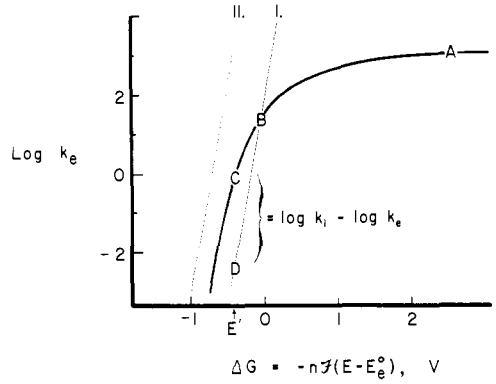

Figure 8. Free energy relationships for electron transfer. Solid heavy curve is the relationship for irreversible electron transfer based on the fit of the Rehm–Weller expression in eq 13. The light lines represent the relationship for reversible electron transfer based on eq 18 with k_2' = 1.2 cm s^{-1} (line I) and $k_2' = 4 \times 10^7$ cm s^{-1} (line II) and are drawn with a slope of unity. For the significance of points A, B, C, and D, see text.

Two features in this analysis must be emphasized. First, the energy difference (error limit) between the intrinsic rate constant k_1 and the experimental rate constant k_e will be less than 0.2 kcal mol^{-1} when the experimental transfer coefficient β_e is less than ~0.7. An inspection of Figure 6 confirms this prediction in that such a small error indeed pertains to all the kinetic situations with driving forces greater than 0.4 V.[41] Second, the error limit is seen in Figure 7 to increase catastrophically for values of β_e greater than ~0.7, and the experimental rate constant k_e may no longer be considered as an adequate reflection of k_1. Consistent with this prediction, the rate constants with values of β_e greater than ~0.7 are readily identified as those existing in the potential region below 0.4 V in Figure 3. This situation arises in Scheme I when the rate of back electron transfer is faster than decomposition, i.e., $k_{-1} \gg k_2'$, and eq 8 simplifies to the relationship: $k_e = k_2'(k_1/k_{-1})$. We consider this kinetic situation to be the *reversible* limit, since under these conditions the functional dependence of the electron-transfer rate constant on the potential is simply given by the Nernstian expression in eq 18.

$$\text{Reversible Case:} \qquad k_e = k_2' \exp\left[\frac{n\mathcal{F}}{RT}(E - E^\circ)\right] \qquad (18)$$

To understand better the utility and limitations of β_e, particularly as an error indicator, let us analyze the general kinetics. In particular, we initially considered two limiting kinetic extremes of reversible and irreversible electron transfer, as indicated by the limits of $k_2'/k_{-1} \ll 1$ and $k_2'/k_{-1} \gg 1$, respectively, for the steady-state expression in eq 8. A reversible electron-transfer process, according to eq 18, is one in which the experimental rate constant ($\log k_e$) will be a linear function of the potential with a unit slope, since the decomposition rate constant k_2' is independent of the applied potential. This kinetic situation has been plotted in Figure 8 as the light lines I and II at two different, arbitrarily chosen values of k_2'. An irreversible electron-transfer process according to eq 15 is one in which k_e will always be equal to k_1. The anticipated response of the electron-transfer rate constant ($\log k_1$) over the extended potential range is indicated by the solid curve in Figure 8, which was drawn on the basis of the Rehm–Weller free energy relationship in eq 13, with $\Delta G_0^\ddagger$ = 6.3 kcal mol^{-1}.[42,43]

(39) (a) The rationale behind this criterion is easily understood with reference to eq 18. According to eq 18, the reversible limit is consistent with only one possible value for β_e, viz., unity. It follows that the further β_e is removed from this benchmark, the higher is the level of confidence with which one can assign the system to the irreversible case. (b) For some relevant examples, see: Saveant, J. M.; Tessier, D. *J. Phys. Chem.* **1978**, *82*, 1723. Andrieux, C. P.; Saveant, J. M. *J. Electroanal. Chem. Interfacial Electrochem.* **1971**, *33*, 453. Březina, M.; Koryta, J.; Loučka, T.; Maršíková, D.; Pradáč, J. *Ibid.* **1972**, *40*, 13. Gileadi, E.; Stoner, G.; Bockris, J. O'M. *J. Electrochem. Soc.* **1966**, *113*, 586. Lines, R.; Utley, J. H. P. *J. Chem. Soc., Perkin Trans. 2* **1977**, 804. Louis, C.; Benoit, R. L. *Electrochim. Acta* **1973**, *18*, 7.

(40) The intrinsic transfer coefficient represents the potential dependence of k_1 in Scheme I.

(41) A referee has queried as to how k_1 and k_e can agree to within 0.2 kcal mol^{-1} at 0.45 V when k_e appears to adhere so closely to the reversible limit between 0.3 and 0.4 V. There is no contradiction, since the transition between reversible and irreversible behavior is expected to be quite rapid (±50 mV), as described by the discussion of the reversibility factor f, in the Experimental Section and Figure 3 in ref 18.

(42) At this juncture, we merely employ the Rehm–Weller eq 13 to provide a functional form of the free energy relationship (see Figure 5b). As a completely empirical relationship, it unfortunately provides no insight into the activation process for electron transfer. (For example, see ref 49.)

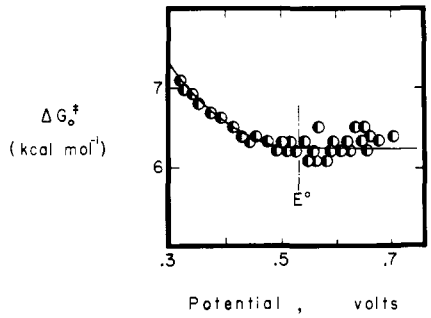

Figure 9. The intrinsic barrier $\Delta G_0^{\ddagger}$ evaluated from the experimental rate constant k_e by using the Rehm–Weller eq 13. Note the deviation of $\Delta G_0^{\ddagger}$ = 6.3 kcal mol^{-1} (represented by the horizontal line) in the endergonic region.

Figure 8 thus depicts the possible behavior of the experimental rate constant k_e in terms of the limiting kinetic situations. Let us now consider the response in the general case. At high values of the driving force, the reverse electron-transfer rate constant k_{-1} slows down according to eq 3 and approaches zero. Therefore, the extreme exergonic region designated by A in Figure 8 always corresponds to the irreversible limit, i.e., $k_2' \gg k_{-1}$. As the value of the applied potential is decreased, the reverse electron-transfer k_{-1} increases, and one proceeds along the solid curve from the irreversible limit until a point is reached at which $k_{-1} = k_2'$. This point occurs at B for the one possible value of k_2' depicted by the light line I (with k_2' = 1.2 cm s^{-1}) in Figure 8. Beyond this point, the system will follow the reversible behavior defined by the line B–D. This simple example underscores two important conclusions. First, large errors in the use of the experimental rate constant k_e (i.e., point D) for the forward rate constant k_1 (point C) at a given driving force of E' can only occur in the endergonic region where the observed slope β_e is large; i.e., the slope B–D is close to unity. Second, the existence of any error at all (i.e., path A–B–D vs. path A–B–C) is critically dependent on the lifetime of the electrogenerated intermediate A^+. Thus when k_2' is sufficiently large (as in the light line II), so that the system always lies in the irreversible region, no error is introduced in equating the experimental rate constant k_e to the intrinsic rate constant k_1.

Criterion for Reversibility in the Experimental Rate Constant k_e and the Determination of k_2'. Since the interpretation of the experimental rate constant k_e in the endergonic region depends on the value of the decomposition rate constant k_2', we deem it desirable to develop some practical criterion as to whether a reversible or irreversible electron transfer applies at a particular value of the driving force. One possible criterion could be based on a limiting value of the transfer coefficient β_e = 1, as predicted by eq 18 for the reversible limit. However we hasten to add that the observation of a slope of unity in the experimental free energy curve as in Figure 3 is not a sufficient condition for reversibility in the electron-transfer step. Thus consider the Rehm–Weller formulation of the free energy relationship in eq 13, which is rewritten as

$$\Delta G^{\ddagger}(\Delta G^{\ddagger} - \Delta G) = \Delta G_0^{\ddagger 2} \qquad (19)$$

to emphasize its hyperbolic form.[44] The asymptotes of $\Delta G^{\ddagger}$ = 0 and $\Delta G^{\ddagger} = \Delta G$ predict the transfer coefficients in the exergonic and endergonic limits to be 0 and 1, respectively. The latter (β = 1) cannot be easily distinguished from the approach to unit slope as a result of the onset of reversibility (i.e., eq 18) in the endergonic region.

A more distinctive approach to this problem involves the measurement of the inherent curvature in the plot of the experimental rate constant (log k_e) over the entire span of free energy change. Since we have shown in Figure 5 that the curvature can be expressed by a single parameter $\Delta G_0^{\ddagger}$ in the Rehm–Weller eq 13 for an irreversible charge transfer, the fit of this parameter is a sensitive test for the occurrence of reversibility in the experimental rate constant. Thus with the aid of eq 13, we reevaluated the intrinsic barrier, this time for each measurement of the *experimental* activation energy $\Delta G^{\ddagger}$ at the particular driving force. The results of these computations are shown in Figure 9. The fact that the entire region cannot be fitted by any single value of $\Delta G_0^{\ddagger}$ verifies the composite nature of the experimental rate constant k_e. Thus, in the exergonic region at the high-potential end, there is no notable trend in $\Delta G_0^{\ddagger}$, which yields a consistent value of 6.3 ± 0.3 kcal mol^{-1}. Since the same value of $\Delta G_0^{\ddagger}$ was determined in Figures 5b and 5c over the entire span of the free energy change, the consistency provides independent verification of the earlier conclusion in eq 15 that the experimental and intrinsic rate constants coincide in the exergonic region. By contrast, in the endergonic region below E° = 0.53 V, there is a clear trend for $\Delta G_0^{\ddagger}$ to increase with diminishing values of the driving force, in a manner similar to that observed for the error function in Figure 6. Such an increasing discrepancy in $\Delta G_0^{\ddagger}$ is thus clearly associated with the onset of reversibility in the electron-transfer step.

To demonstrate that the method provides a rigorous test for reversibility, we apply the converse argument to show how it can be used to evaluate the decomposition rate constant k_2' from a knowledge of k_e. We proceed as follows. First, the rate data in the exergonic region with $\beta_e < 0.7$ (i.e., path A–B in Figure 8) is used to evaluate E° and $\Delta G_0^{\ddagger}$ by fitting them to the Rehm–Weller expression. Second, the knowledge of E° and $\Delta G_0^{\ddagger}$ is sufficient to calculate the intrinsic rate constant k_1 in the endergonic region where $\beta_e > 0.7$ (i.e., path B–C in Figure 8. Note that this differs from path B–D, which corresponds to the experimental rate constant k_e in the endergonic region.). Third, the calculated values of k_1, the experimental values of k_e, and the standard potential E° (see the next section) are used in conjunction with eq 20 (which is the rearranged form of eq 10) to determine

$$k_2' = k_1 k_e \exp\left[-\frac{n\mathcal{F}}{RT}(E - E^\circ)\right] \Big/ (k_1 - k_e) \qquad (20)$$

the decomposition rate constant k_2' at various potentials in the endergonic region. The results of the computations are listed in the last column of Table II after conversion to the homogeneous counterpart k_2.[31,45] It is noteworthy that the value of k_2 deter-

Table II. Decomposition Rate Constant (k_2) Determined from the Wave Shape Analysis of Irreversible Electrochemical CV Data[a]

v, V s^{-1} [b]	E, V[c]	log k_e, cm s^{-1}	log k_1, cm s^{-1} [d]	log k_2, s^{-1} [e]
0.03	0.318	−3.6800	−3.2254	5.0
0.03	0.347	−3.2700	−2.8962	5.0
0.03	0.373	−2.8900	−2.6105	5.0
0.03	0.399	−2.5600	−2.3341	4.9
0.06	0.358	−3.0600	−2.7743	5.2
0.10	0.368	−2.9300	−2.6648	5.1
0.30	0.346	−3.2100	−2.9074	5.2
0.30	0.383	−2.7200	−2.5031	5.2
0.60	0.361	−2.9100	−2.7413	5.3
1.00	0.377	−2.7900	−2.5674	5.2
3.00	0.368	−2.7800	−2.6648	6.0

[a] In acetonitrile solution containing 0.1 M tetraethylammonium perchlorate at 25 °C. [b] Sweep rate. [c] Applied potential vs. saturated NaCl SCE. [d] Calculated from eq 11 and 13. [e] From eq 20 and the relationship in ref 31.

(43) (a) The inherent curvature in the plot of the activation free energy in Figure 8 is determined by the parameter $\Delta G_0^{\ddagger}$. (b) For a discussion of curvature in free energy relationships, see: ref 2, Balzani, F.; Bolletta, F.; Scandola, F. *J. Am. Chem. Soc.* **1980**, *102*, 2153, and Agmon in ref 7d.

(44) For the hyperbolic form of free energy relationships, see a discussion by: Lewis, E. S.; Shen, C. C.; More O'Ferrall, R. A. *J. Chem. Soc., Perkin Trans. 2* **1981**, 1084.

(45) (a) For the calculations, values of $\Delta G_0^{\ddagger}$ = 6.3 kcal mol^{-1}, E° = 0.53 V, and the data in Table I were used. The principal error in this type of analysis is expected to result from locating the potential at which $\beta_e = {}^1/_2$. Thus an uncertainty of 30 mV in E_e° (compare Figure 9) results in an error of one order of magnitude in k_2. (b) Note that this analysis provides a generally useful method for measuring the decomposition rate constants k_2', which would otherwise be very difficult to evaluate.

mined in this manner is in striking agreement with $k_2 = 10^5\ s^{-1}$, which was previously measured by a completely independent kinetic technique.[19,46]

Determination of E° for Irreversible Electron Transfer. The construction of a free energy curve requires knowledge of the standard potential, which is often difficult to measure in an irreversible process. We wish to show how the curvature in the potential dependence of the experimental rate constant (log k_e) can be used to define a unique value of the standard free energy change for outer-sphere electron transfer. In a recent study we established the direct relationship between heterogeneous electrochemical and homogeneous chemical electron transfer in a series of organometal donors.[49] The curvature in the activation free energy relationship was shown to be a property inherent to the electron-transfer process. Indeed the curvature is independent of the experimental means for determining it, whether the method be electrochemical or chemical. This inherent curvature can be used to define a unique value of the experimentally measureable free energy change. In particular, we choose ΔG at the observed slope where β_e is equal to $^1/_2$. In other words, from the relationship

$$\Delta G = -n\mathcal{F}(E - E_e^\circ) \qquad (21)$$

E_e° is defined to be the potential E at which $\beta_e = {}^1/_2$. For $Me_2Co(DpnH)$ in Figure 3 it is 0.53 V.[50]

Having defined E_e° in terms of the experimentally measureable parameters, it is important to address the theoretical significance of this quantity. We begin by noting that the free energy relationship based on the Rehm–Weller expression in eq 13 coincides with that based on the Marcus theory for systems in the region close to the equilibrium potential.[38b] Owing to its theoretical significance, it is advantageous to carry out the further analysis of E_e° in terms of the Marcus theory.[1-3] According to eq 12, the activation free energy $\Delta G^\ddagger$ for outer-sphere electron transfer relates to the standard free energy change ($\Delta G + w^p$) through an intrinsic barrier $\Delta G_0^\ddagger$, where w^p is the work needed to bring the products together, or bring the product to the electrode.[51] (For neutral reactants such as $Me_2Co(DpnH)$, we consider the work term w^r to be nil.[52]) The Marcus theory predicts a quadratic dependence of the activation free energy $\Delta G^\ddagger$ on the thermodynamic driving force. Notably eq 12 predicts a slope of $^1/_2$ at ($\Delta G + w^p$) = 0, and this prediction has been verified in numerous examples.[15,53] Although the experimental dependence in Figure 4 is more complicated than the simple parabolic shape predicted by eq 12, the point at which β_e is equal to $^1/_2$ is unique. Therefore if the Marcus theory applied to $Me_2Co(DpnH)$, the experimentally measureable parameter E_e° must have the value given by eq 22, where $w^{p\prime} =$

$$E_e^\circ = E^\circ + (n\mathcal{F})^{-1}[w^p + 4w^{p\prime}\Delta G_0^\ddagger/(1 + w^{p\prime})] \qquad (22)$$

$\partial w^p/\partial \Delta G$. Equation 22 predicts that E_e° will only differ from the standard reduction potential E° by the function of the work term in the brackets. Provided there is no specific interaction with the electrode surface, the outer-sphere work terms are expected to be small and may be approximated by appropriate electrostatic models.[54] The question of the specific interaction with the electrode has been resolved in this organometal system since the direct correspondence of the electrochemical and chemical rate constants has demonstrated a common outer-sphere mechanism for these oxidations.[49]

Summary and Conclusion

The experimental rate constants k_e for outer-sphere electron transfer in Figure 3 span the extended range of free energy changes from the exergonic to the endergonic limits. With regard to the generalized kinetic Scheme I, the *exergonic region* is characterized by (i) the experimental rate constant k_e, which approaches the intrinsic rate constant k_1, (ii) the transfer coefficient, which approaches a limiting value $\beta_e = 0$, and (iii) the rate constant $k_2' \gg k_{-1}$, which also makes it the irreversible kinetic limit. The *endergonic limit* is characterized by (a) the experimental rate constant k_e, which approaches $k_2'(k_1/k_{-1})$, (b) the transfer coefficient, which reaches a limiting value of $\beta_e = 1$, and (c) the rate constant $k_{-1} \gg k_2'$, which also makes it the reversible kinetic limit.

The transfer coefficient β_e uniquely defines the irreversible limit in the exergonic region; i.e., $\beta \to 0$ is concurrent with $k_{-1}/k_2' \to 0$. In particular, those portions of the experimental free energy curve that exhibit β_e less than 0.7 may be assigned to the irreversible kinetic limit for electron transfer (i.e., eq 15). They yield experimental rate constants (log k_e) that agree with the intrinsic rate constant (log k_1) to within 0.2 kcal mol^{-1} (Figure 6).

The utility of β_e as a measure of the irreversibility in the electron-transfer step diminishes as it approaches 1 in the endergonic region, as indicated by the error limits in Figure 7. Indeed the limiting value of $\beta = 1$ is equally consistent with either reversible or irreversible electron transfer, as illustrated in Figure 8. Fortunately with $Me_2Co(DpnH)$, the availability of an independent determination of the decomposition rate constant k_2' provides the necessary information to analyze the kinetics in the endergonic region. Thus the intrinsic rate constant k_1 can be expressed analytically as a function of the experimental rate constant k_e by explicitly taking into account reversibility according to eq 10. The intrinsic rate constant (log k_1) obtained in this manner is shown in Figure 5 to fit the Rehm–Weller and Marcus–Levine–Agmon free energy relationships over the entire span of the driving force with a single value of the intrinsic barrier, $\Delta G_0^\ddagger = 6.3$ kcal mol^{-1}. Thus the experimental transfer coefficient β_e in the endergonic region reflects both electron-transfer reversibility as well as the potential dependence of the intrinsic rate constant (log k_1), the relative importance of each depending on the value of k_2'.[55] By utilizing this interdependence, a method is outlined that analyzes the experimental free energy curve to allow the decomposition rate constant k_2' to be evaluated in Table II.

(46) Such a lifetime is generally determined for systems in which both the anodic and cathodic CV waves can be observed by a standard analysis of the sweep rate of the current–potential function.[47,48] However, for systems such as $Me_2Co(DpnH)$, which exhibit irreversible CV waves of the type shown in Figure 1, this type of analysis is impossible. Fortunately, this problem may be resolved by the appropriate combination of chemical and electrochemical techniques. For example, the electrolysis of $Me_2Co(DpnH)$ at constant current provides a well-defined flux of methyl radicals whose kinetics may be examined by the competition method with suitable chemical trapping methods. See ref 19 for details.

(47) Nicholson, R. S.; Shain, I. *Anal. Chem.* **1964**, *36*, 706.

(48) MacDonald, D. D. "Transient Techniques in Electrochemistry"; Plenum: New York, 1977.

(49) Klingler, R. J.; Kochi, J. K. *J. Am. Chem. Soc.* **1981**, *103*, 5839.

(50) The values of E_e° can also be extracted from routine CV data of irreversible systems by the straightforward procedures described in the Experimental Section. The procedure is mathematically equivalent to drawing chords between data points of log k_e in Figure 3 and plotting the resultant slopes against the applied potential. A value of $E_e^\circ = 0.52$ V is obtained in Figure 10 in the Experimental Section.

(51) For the discussion of the work terms, see the discussion by: Mohilner, D. M. *J. Phys. Chem.* **1969**, *73*, 2652. Note that in eq 12, w^p was not included in the free energy change. See ref 54.

(52) (a) The work term of the reactants is omitted in eq 12, since it is taken as zero for the neutral reactants such as $Me_2Co(DpnH)$, as described in ref 19. (b) See ref 14 and 34.

(53) (a) The slope is actually $^1/_2 + w^{p\prime}$, but $w^{p\prime} \sim 0$ (see ref 34). (b) For leading references, see: Sutin, N. In "Inorganic Biochemistry"; Eichhorn, G. L., Ed.; Elsevier: Amsterdam, 1973; Vol. II, p 611 ff, and ref 8 and 15. Hale, J. M. In "Reactions of Molecules at Electrodes"; Hush, N. W., Ed.; Wiley: New York, 1971, p 229.

(54) (a) Since both work terms are small for these systems (see ref 49), we have employed E_e° as equal to E° throughout this study. The assumption that the work terms in this system are small is strongly supported by the direct comparison of the heterogeneous electrochemical rate data with the homogeneous chemical rate data, as described in ref 13b, 19, and 49. (b) Calculations based on a dielectric continuum model have been typically for electron transfer in homogeneous systems. (See Marcus in ref 1 and Brown, G. M.; Sutin, N. *J. Am. Chem. Soc.* **1979**, *101*, 883.) In heterogeneous electrochemical systems, the dielectric continuum model of Gouy–Chapman (as modified by Stern for the finite size of the ionic radius of the supporting electrolyte) has been often used. See ref 9b and 10b.

(55) For example, the error function arising from electron-transfer reversibility in Figure 6 is ~1 kcal mol^{-1} at 0.3 V for $Me_2Co(DpnH)$. Thus most of the slope in Figure 3 at this potential arises from the potential dependence of the intrinsic rate constant shown in Figure 4.

Table III. Measurement of the Uncompensated Cell Resistance[a]

ω, Hz	i, μA	Z, Ω
1	1.15	83000
10	7.2	14000
100	50	2000
1000	370	270
10000	2500	34

[a] See text for definitions.

The experimental free energy relationship includes the point where $E = 0.53$ V, at which the transfer coefficient β_e is equal to $^1/_2$. To interpret the theoretical significance of ΔG, we turn to the Marcus theory, which states that $\Delta G = -n\mathcal{F}(E - E_e^\circ)$, where E_e° is the standard reduction potential E° plus the work terms, which are small for the outer-sphere process examined in this study. Thus at $\beta_e = ^1/_2$, E is defined to be E_e° and $\Delta G = 0$. The intrinsic barrier $\Delta G_0^\ddagger$ can be evaluated at this point, or more equitably by the use of the kinetic data (log k_1) over the entire free energy span by using the free energy relationships, as in Figure 5. The cyclic voltammetric determination of the transfer coefficient at $\beta_e = ^1/_2$ also provides a convenient method to evaluate the standard reduction potentials for irreversible systems (see Figure 10 in the Experimental Section).

Experimental Section

Materials. The preparation of $Me_2Co(DpnH)$ was described previously.[19] Reagent grade acetonitrile (Fisher Chemical Co.) was further purified by refluxing it over calcium hydride, then treated with potassium permanganate, and redistilled from P_2O_5 through a 19-plate bubble cap Oldershaw column. Tetraethylammonium perchlorate (TEAP) was obtained from the G. F. Smith Chemical Co. and dried in vacuo at 60 °C.

Electrochemical Measurements. Electrochemistry was performed on a Princeton Applied Research Model 173 potentiostat equipped with a Model 176 current-to-voltage converter that provided a feedback compensation for ohmic drop between the working and reference electrodes. The high impedance voltage follower amplifier (PAR Model 178) was mounted external to the main potentiostat to minimize the length of the connection to the reference electrode. This arrangement ensured low noise pickup. Cyclic voltammograms were recorded on a Houston Series 2000 X-Y recorder. The electrochemical cell was constructed according to the design of Van Duyne and Reilley.[56] The distance between the platinum working electrode and the tip of the salt bridge was 1 mm to minimize ohmic drop. The performance of the electrochemical systems was initially tested by applying a 100-mV peak-to-peak sinusoidal wave and measuring the resultant ac current with a PAR Model 5203 lock-in amplifier. The current i measured at various frequencies ω is listed in Table III. Extrapolation of the observed impedance Z to infinite frequency (i.e., ω^{-1} extrapolated to zero) establishes an upper limit of 2 ohms for the uncompensated cell resistance. Digital current–time data for the convolution linear sweep voltammetry were recorded on a Princeton Applied Research Model 4102 transient signal recorder. The signal recorder was interfaced to a Digital Equipment Corp. PDP 11/23 computer. All computations were performed on this system.

Convolutive Potential Sweep Voltammetry. All electrochemical measurements were carried out at 25 °C in acetonitrile solutions, with 0.26 M tetraethylammonium perchlorate as supporting electrolyte. The platinum electrode was initially cleaned by soaking it in concentrated nitric acid for 1 h, followed by repeated rinsing with distilled water and drying at 120 °C prior to use. In between each scan, the electrode was cleaned with a fine polishing cloth, as described below. In addition, the cracked-tip salt bridge was stored in a solution of acetonitrile that was 0.26 M in TEAP when not in use. Under these conditions the day-to-day reproducibility of the peak potential measurements at 100 mV s^{-1} was ±10 mV.

During a typical experiment, the electrochemical cell was filled with a solution of acetonitrile containing only 0.26 M TEAP. The applied potential was alternately stepped to −2.0 V vs. SCE for 5 s and then returned to 0.0 V sequentially 3 times in succession. The latter procedure was found to improve the reproducibility of the background charging current. The charging current was recorded at least twice, and checked to be reproducible to within ±5% by a comparative procedure utilizing the two memories of the transient signal recorder. The dwell time for sampling the current was optimized between 50 ms and 25 μs to obtain up to 1000 data points per sweep. The solution was gently drained through the bottom of the cell and replaced with a 2.12×10^{-3} M solution of $Me_2Co(DpnH)$ in acetonitrile (0.26 M in TEAP). The current data were recorded again at least twice, and checked to be reproducible to within ±5%. In between runs, the cell was cleaned with an acetonitrile solution containing 0.26 M in TEAP, and the electrode was buffed with a fine polishing cloth.

The convolution integral, $\Psi(t)$ in eq 23, is related to the time-dependent concentration in eq 7:

$$\Psi(t) = \frac{10^3}{n\mathcal{F}AC^0(\pi D)^{1/2}} \int_0^t i(\eta)(t - \eta)^{-1/2}\, d\eta \qquad (23)$$

$$C(t) = C^0[1 - \Psi(t)] \qquad (24)$$

The convolution integral, $\Psi(t)$, was evaluated by conversion to the finite summation in eq 25, where θ is the dwell-time interval between the data points, and m is the number of subintervals within the time period t defined according to $m = t/\theta$. The current i_{m-n} is evaluated at the time $\theta(m - n)$, and the coefficients a_n are obtained according to the relationship

$$\Psi(t) = (\theta/\pi)^{1/2} \sum_{n=0}^{m} a_{n+1} i_{m-n} \qquad (25)$$

$$a_n = (4n\sqrt{n} + (8 - 8n)\sqrt{n-1} + (4n - 8)\sqrt{n-2})/3 \qquad (26)$$

which only applies for $n > 1$ (note: $a_1 = ^4/_3$). Integration with the coefficients defined by eq 26 is exact if the current can be considered to be a linear function of the time within the subintervals of length θ. This will always be true for a sufficiently short time interval. In practice, the values obtained from eq 26 were found to be rather insensitive to the coarseness of the time grid θ, provided the wave was divided into at least 20 intervals. The resultant convolution integral–time data were converted into the corresponding convolution integral–potential set by noting that $E = E_i + vt$, where E_i and v are the initial potential and the sweep rate, respectively. Finally, the area of the electrode was determined from the limiting value Ψ_L of the convolution integral, in which case eq 6 (see Results) reduces to

$$k_e(E) = D^{1/2} i(E)/(\Psi_L - \Psi_E) \qquad (27)$$

as discussed by Imbeaux and Saveant.[27] The FORTRAN program for evaluating eq 25–27 was tested with the theoretical current–potential data tabulated by Nicholson and Shain[47] for a totally irreversible CV wave, and it is available upon request.

Determination of E_e° for the Log k_e Data. Examination of Figure 3 indicates that the experimental slope varies smoothly from 0.9 to 0.3. However, despite the determination of over 1500 rate constant data, there is still sizeable scatter in the result. This scatter will be greatly magnified by any numerical differentiation process. The analysis of Figure 5 indicates that the two-parameter Rehm–Weller equation empirically fits the data for values of the applied potential greater than 0.44 V. Therefore, this equation was used to determine the point at which the slope is 0.5 by the following procedure: First, an E_e° value of 0.55 V was graphically estimated and used to calculate a set of $\Delta G_0^\ddagger$ values as described in the text. These $\Delta G_0^\ddagger$ values were averaged and used to calculate the point at which the slope was $^1/_2$. The calculations carried out by this procedure provided a better estimate of E_e° from the rate constant data. This process was repeated until a consistent pair of $E_e^\circ = 0.53 \pm 0.01$ and $\Delta G_0^\ddagger = 6.3 \pm 0.05$ were obtained for Figure 3.

Determination of E_e° from Current–Potential Data. As discussed previously,[18] the location of the current peak in the CV experiment for a totally irreversible system corresponds to a measurement of the electron-transfer rate constant k_e according to[57]

$$k_e \text{ (at } E_p) = 2.18(D\beta n\mathcal{F}v/RT)^{1/2} \qquad (28)$$

where v is the sweep rate. An analogous equation exists for the half-peak potential $E_{p/2}$:[58]

$$k_e \text{ (at } E_{p/2}) = 0.34(D\beta n\mathcal{F}v/RT)^{1/2} \qquad (29)$$

Consideration of eq 28 and 29 indicates that the experimental location

(56) Van Duyne, R. P.; Reilley, C. N. *Anal. Chem.* **1972**, *44*, 142.

(57) This conclusion is not completely unexpected, since the CV method summarized by eq 28 can be derived from eq 6. Thus Nicholson and Shain[47] have shown for linear sweep voltammetry that the current peak i_p will occur when the concentration $C(t)$ has dropped to 22.7% of C^0. Proceeding from eq 6, it then follows that $k_e(E_p) = (n\mathcal{F}A)^{-1} i_p/0.227C^0$, which is identical with eq 28 since the peak current is given by[47] $i_p = 0.4958\, n\mathcal{F}AC^0(Dn\mathcal{F}v/RT)^{1/2}$.

(58) Defined as that potential at which the current is $^1/_2$ the peak current i_p.

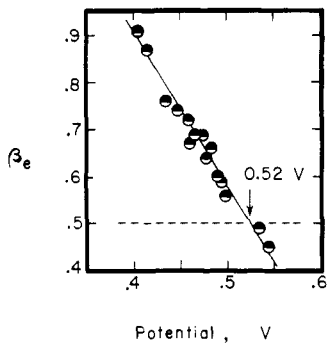

Figure 10. The dependence of the experimental transfer coefficient β_e on the applied electrode potential E for $Me_2Co(DpnH)$ in CH_3CN containing 0.26 M TEAP at 25 °C.

of the peak potential E_p and the half-peak potential $E_{p/2}$ corresponds to the determination of a chord between two points in the rate data shown in Figure 3. Simple rearrangement of eq 28 and 29 yields the result originally given by Nicholson and Shain,[47] i.e.:[59]

$$\beta_e = \frac{1.857RT}{n\mathcal{F}}(E_p - E_{p/2})^{-1} \tag{30}$$

The values of β_e thus obtained are plotted against the average of $(E_p + E_{p/2})/2$ in Figure 10. The value at which the observed transfer coefficient β_e equals $^1/_2$, viz., $E_e^\circ = 0.52 \pm 0.01$, is readily obtained by this procedure and compares quite favorably with that obtained from analysis of the rate constant data in Figure 3.

Reversibility Factor f_r and Electrochemical Kinetics of Scheme III. The electrochemical problem in cyclic voltammetry is readily described on the basis of the simple kinetic Scheme III, which is a more detailed electrochemical form of Scheme I, where the subscripts 0 and s refer to the concentrations at the electrode surface and in the bulk solution, respectively. In the usual situation, the electrochemical current corresponds to the difference between the rate of the forward electron transfer and that of the reverse step, as given in eq 34. The concentration of the intermediate $[A_0^+]$ is given in terms of the rate constants in Scheme III as

Scheme III

$$A_0 \underset{k_{-1}}{\overset{k_1}{\rightleftharpoons}} A_0^+ \tag{31}$$

$$A_0^+ \xrightarrow{k_d} A_s^+ \tag{32}$$

$$A_0^+ \xrightarrow{k_r} B_s \tag{33}$$

$$i/n\mathcal{F}A = k_1[A_0] - k_{-1}[A_0^+] \tag{34}$$

$$[A_0^+] = [A_0]k_1/(k_{-1} + k_2') \tag{35}$$

where $k_2' = k_r + k_d$.[60] The validity of eq 35 (which is tantamount to a steady-state kinetic analysis) has been verified by the rigorous solution of the inhomogeneous kinetics described in Scheme III.[29] The combination of eq 6 with eq 34 and 35 yields the expression for the net forward rate constant in terms of the fundamental kinetic parameters in Scheme III as

$$k_e = k_1k_2'/(k_{-1} + k_2') \tag{36}$$

In the CV experiment, total irreversibility can be achieved by (1) enhancing the chemical reactivity of the electrogenerated intermediate A_0^+ (i.e., increasing k_r in eq 33) and/or (2) increasing the rate of mass transport of A_0^+ from the electrode surface by the variation in the sweep rate (i.e., k_d in eq 32).[17]

Electrochemical reversibility in cyclic voltammetry has been discussed in terms of the reversibility factor f_r in eq 37 as that fraction by which the concentration ratio of the electroactive species (A_0 and A_0^+ in Scheme III) has been reduced from the value predicted by the Nernst equation, i.e.,[18]

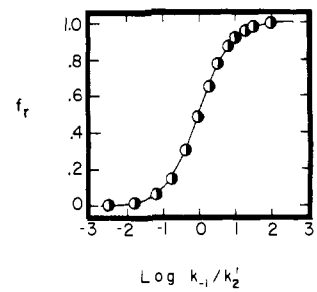

Figure 11. Variation of the reversibility factor f_r as a function of the rate constant ratio k_{-1}/k_2'.

$$\frac{[A_0^+]}{[A_0]} = f_r \exp\left[\frac{n\mathcal{F}}{RT}(E - E^\circ)\right] \tag{37}$$

Defined as such, f_r varies smoothly between the limits of unity and zero for the limiting kinetic situations described above as reversible and totally irreversible, respectively. The reversibility factor f_r is directly related to the intrinsic kinetic parameters in Scheme III according to eq 38. Figure

$$\frac{f_r}{1 - f_r} = \frac{k_{-1}}{k_2'} \tag{38}$$

11 illustrates how the reversibility factor is a smooth function of the rate constant ratio k_{-1}/k_2'.

Let us now consider how the magnitude of the reversibility factor defines the reversible and irreversible limits of electron transfer for the kinetics in Scheme III.

A. Reversible Electron Transfer. As the reversibility factor f_r approaches unity, the observed rate constant for net electron transfer will approach the functional form given by eq 39, which derives from a consideration of eq 36 and 38, with $k_{-1} \gg k_2'$.

$$k_e = k_2' \exp\left[\frac{n\mathcal{F}}{RT}(E - E^\circ)\right] \tag{39}$$

Since k_2' is independent of the applied potential, eq 39 predicts the observed rate constant ($\log k_e$) to be a linear function of E with a slope of unity. Inspection of the experimental results in Figure 3 indicates such a prediction is borne out only in the highly endergonic region—the deviation from a unit slope is increasing, especially at the larger values of the applied potential. Thus the oxidation of $Me_2Co(DpnH)$ does not conform to a reversible Nernstian couple over the potential range of 0.3–0.8 V vs. SCE in Figure 3. It is just this deviation from reversible behavior that allows the determination of the intrinsic rate constant k_1 for heterogeneous electron transfer.

B. Irreversible Electron Transfer. As the reversibility factor f_r approaches zero, the observed rate constant for net electron transfer will become equal to the forward rate constant k_1, which derives from a consideration of eq 36 and 38, with $k_2' \gg k_{-1}$. In this limit, the slope of the free energy relationship in Figure 3 represents the electrochemical transfer coefficient β, i.e.,

$$\beta_e = \frac{2.3RT}{n\mathcal{F}}\left(\frac{\partial \log k_e}{\partial E}\right) = \frac{2.3RT}{n\mathcal{F}}\left(\frac{\partial \log k_1}{\partial E}\right) = \beta \tag{40}$$

The measured value of the transfer coefficient β_e and the true β for the intrinsic rate constant coincide at this irreversible limit.

C. Comparison of the Rate Constants k_2' and k_{-1}. An important feature in Figure 11 is the rapid transition between reversible and irreversible behavior that occurs in the region centered about the point at which $k_2' = k_{-1}$. Thus the variation of only 0.43 in $\log (k_{-1}/k_2')$ corresponds to a decrease of the reversibility factor $f_r = 0.75$ to 0.25. Systems that exhibit $f_r < 0.25$ may be assigned to the irreversible case (eq 15) with a confidence level of 0.2 kcal mol^{-1}.[18] On the basis of eq 3, the variation of $\log (k_{-1}/k_2') = 0.43$ is expected to occur within a potential region of 50 mV, assuming an average transfer coefficient β of 0.5 for the general case. In the $Me_2Co(DpnH)$ system, k_2' has been evaluated as 1.2 cm s^{-1}.[19] While k_{-1} is not directly measured, it may be calculated from the values of k_1 listed in Table I and the Nernst equation with $E^\circ = 0.53$ V to have the value of 1.2 cm s^{-1} at $E = 0.36$ V. Thus the transition in the reversibility factor from $f_r = 0.75$ to 0.25 is expected to occur in Figure 9 over a rather limited region of the applied potential between 0.31 and 0.41 V. This is graphically demonstrated by the marked curvature

(59) This analysis assumes the transfer coefficient to be effectively a constant over the width of the CV wave, an operation that is similar to drawing chords between individual data points in Figure 3.

(60) The appropriate conversion of the heterogeneous rate constant k_r to the homogeneous chemical rate constant κ is given by $k_r = (D\kappa)^{1/2}$, and the transport rate constant k_d (in cm s^{-1}) due to planar diffusion in linear sweep voltammetry is given by $k_d = 2.82\ (nDv)^{1/2}$ where D is in units of cm^2 s^{-1} and v in V s^{-1}. See ref 31.

of the plot in the potential region below 0.4 V in Figure 9, which is notably absent in the plot derived from the complete kinetic situation presented in Figure 5a.

Peak Broadening of the CV Wave and the Nature of the Electrochemical Reversibility. In the kinetics of Scheme III, the disappearance of the electrogenerated intermediate A_0^+ depends on the overall rate constant k_2'. Actually, two pathways exist for the depletion of A_0^+, viz., the diffusion rate constant k_d in eq 32 and the chemical reaction rate constant k_r in eq 33.

Diffusion is known to be proportional to the square root of the sweep rate,[24] whereas k_r will be a constant that is specific to the chemical system, i.e., the chemical identity of A_0^+. Both processes operate simultaneously in the inhomogeneous concentration profile extant at the electrode surface. Nonetheless, it has been shown that the net effect k_2' may be described as a simple sum of the two rate processes, i.e.,[18,60]

$$k_2' = k_r + k_d \tag{41}$$

The results in Figure 2 indicate that the net forward rate constant k_e in eq 36 is independent of the sweep rate varying over 4 orders of magnitude. This is consistent with the generation of a highly unstable intermediate in which k_2' is dominated by k_r over the entire range of accessible sweep rates.[61] This result has important implications. Thus, the CV waves in Figure 1 are observed to broaden (as measured by $E_p - E_{p/2}$) substantially at higher sweep rates. This broadening is not due to a decrease in the electrochemical reversibility.[62] For example, if k_2' were controlled by k_d, the maximum slope of the plot of log k vs. log v would be 0.5 for systems in which electrochemical reversibility (as defined by eq 37 and 38) is determined by the sweep rate.

Furthermore, we can conclude that the broadening of the CV waves in Figure 1 is not due to an experimental artifact such as an uncompensated cell resistance.[63] Thus at any constant value of the applied potential, the current increases as the square root of the sweep rate. Yet the value of the measured rate constant is invariant, as shown by the horizontal rows in Figure 2. Therefore, uncompensated iR drops have a minimal influence on the rate data. Indeed, the slopes in Figure 2 in conjunction with eq 42 may be used to estimate an upper limit on the uncompensated cell resistance,

$$\mathrm{d} \log k_e = (\beta n \mathcal{F}/2) V_{cell}\, \mathrm{d} \log v \tag{42}$$

where $V_{cell} = iR_{cell}$. Since the slopes in Figure 2 are all close to zero, the uncompensated cell resistance must also be close to zero, according to eq 42. Indeed, this conclusion accords well with the results obtained from Table III.

We can thus conclude that the broadening of the CV waves with sweep rate is not due to (1) changes in degree of electrochemical reversibility or (2) experimental artifacts such as uncompensated cell resistance. However, such a peak broadening could result directly if the transfer coefficient β_e were itself a function of the applied potential. Thus standard electrochemical theory indicates that the width of the CV wave will be given by eq 30. Indeed the plot of k_e vs. E in Figure 3 indicates a substantial degree of curvature, consistent with a potential dependence of β.[49]

Acknowledgment. We wish to thank the National Science Foundation for support of this research and funds to purchase the electrochemical equipment and the computer and Professor C. Walling for helpful comments of the manuscript.

Registry No. $Me_2Co(DpnH)$, 33569-60-7.

Supplementary Material Available: Tabulation of the experimental rate constants k_e and electrochemical data used (27 pages). Ordering information is included on any current masthead page.

(61) In other words, the electrochemical irreversibility induced by the fast following chemical reaction is already so large that the reversibility of the system cannot be significantly altered, even by employing sweep rates as high as 1000 V s^{-1}.

(62) The interpretation of the broadening and concurrent shifting of the CV wave as due to changes in the electrochemical reversibility of the system while a constant value of the transfer coefficient is maintained is the basis of the method proposed by Nicholson[63] for obtaining the data for heterogeneous rate constants.

(63) The broadening effect of CV waves arising from uncompensated cell resistance is known. See: Nicholson, R. S. *Anal. Chem.* **1965**, *37*, 1351.

Micellar Photochemistry. Photooxidations with Intramicellar-Generated Singlet Oxygen

Michael C. Hovey

Contribution No. 2958 from Central Research and Development Department, Experimental Station, E. I. du Pont de Nemours & Company, Wilmington, Delaware 19898.
Received October 14, 1981

Abstract: Pyrex-filtered irradiation of an aerated 5% aqueous sodium dodecyl sulfate ($NaDodSO_4$) solution of 2.8 mM 10-methylphenothiazine (MPT) and 2.8 mM benzyl sulfide resulted in formation of a 39% yield of benzyl sulfoxide. The reaction was general for transformation of a variety of sulfides to sulfoxides and for triphenylphosphine to triphenylphosphine oxide and was catalytic with respect to MPT. Also effective in promoting the photooxidation were 10-acetylphenothiazine, 10-benzoylphenothiazine, 10-(2-cyanoethyl)phenothiazine, 10-methyl-2-(trifluoromethyl)phenothiazine, and 3-bromo-10-methylphenothiazine. The photooxidation also took place in microemulsion media. Singlet oxygen was implicated as the primary oxidizing agent and is thought to arise by the intramicellar recombination of the transient $MPT^{+\cdot}/O_2^{-\cdot}$ ion pair. The rates of quenching of $^1O_2$ by benzyl sulfide and MPT were measured in chloroform solution. The quenching rate, k_Q, was 6.4×10^6 M^{-1} s^{-1} for benzyl sulfide and 2.9×10^6 M^{-1} s^{-1} for MPT. The reaction of singlet oxygen with benzyl sulfide in the presence of MPT in the micelle was discussed in terms of the greater tendency of the MPT to quench singlet oxygen rather than react to form 10-methylphenothiazine 5-oxide.

Aqueous micellar medium effects on photophysical processes have seen much attention recently.[1] The use of micelles to promote synthetically useful photochemical reactions is an area of rapidly increasing interest. Some examples of synthetic reactions include photocycloadditions,[2] substitutions,[3] isotopic enrichment,[4] and remote functionalization.[5] In contrast to those in homogeneous solution, products and yields often change dra-

(1) J. K. Thomas, *Chem. Rev.*, **80**, 283-299 (1980).

(2) (a) K.-H. Lee and P. de Mayo, *J. Chem. Soc., Chem. Commun.*, 493-495 (1979); (b) Y. Nakamura, Y. Imakura, T. Kato, and Y. Morita, *ibid.*, 887-888 (1977); (c) Y. Nakamura, Y. Imakura, and Y. Morita, *Chem. Lett.*, 965-968 (1978).

(3) (a) R. R. Hautala and R. L. Letsinger, *J. Org. Chem.*, **36**, 3762-3768 (1971); (b) J. B. S. Bonilha, H. Chaimovich, V. G. Toscano, and F. Quina, *J. Phys. Chem.*, **83**, 2463-2470 (1979).

(4) (a) N. J. Turro, B. Kraeutler, and D. R. Anderson, *J. Am. Chem. Soc.*, **101**, 7435-7437 (1979); (b) *Tetrahedron Lett.*, 3-6 (1980); (c) B. Kraeutler and N. J. Turro, *Chem. Phys. Lett.*, **70**, 266-269 (1980).

(5) (a) R. Breslow, S. Kitabatake, and J. Rothbard, *J. Am. Chem. Soc.*, **100**, 8156-8160 (1978); (b) M. Mitani, T. Suzuki, H. Takeuchi, and K. Koyama, *Tetrahedron Lett.*, 803-804 (1979).

0002-7863/82/1504-4196$01.25/0